
This is an electronic reprint of the original article.
This reprint may differ from the original in pagination and typographic detail.

Reijonen, Joni; Björkstrand, Roy; Riipinen, Tuomas; Que, Zaiqing; Metsä-Kortelainen, Sini; Salmi, Mika

Cross-testing laser powder bed fusion production machines and powders

Published in:
Materials & Design

DOI:
[10.1016/j.matdes.2021.109684](https://doi.org/10.1016/j.matdes.2021.109684)

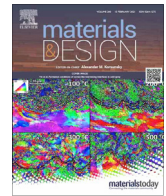
Published: 01/06/2021

Document Version
Publisher's PDF, also known as Version of record

Published under the following license:
CC BY

Please cite the original version:
Reijonen, J., Björkstrand, R., Riipinen, T., Que, Z., Metsä-Kortelainen, S., & Salmi, M. (2021). Cross-testing laser powder bed fusion production machines and powders: Variability in mechanical properties of heat-treated 316L stainless steel. *Materials & Design*, 204, Article 109684. <https://doi.org/10.1016/j.matdes.2021.109684>

This material is protected by copyright and other intellectual property rights, and duplication or sale of all or part of any of the repository collections is not permitted, except that material may be duplicated by you for your research use or educational purposes in electronic or print form. You must obtain permission for any other use. Electronic or print copies may not be offered, whether for sale or otherwise to anyone who is not an authorised user.



Cross-testing laser powder bed fusion production machines and powders: Variability in mechanical properties of heat-treated 316L stainless steel



Joni Reijonen^{a,*}, Roy Björkstrand^b, Tuomas Riipinen^a, Zaiqing Que^c, Sini Metsä-Kortelainen^a, Mika Salmi^b

^aVTT Technical Research Centre of Finland Ltd., Advanced Manufacturing Technologies, Kemistintie 3, Espoo 02150, Finland

^bAalto University, Department of Mechanical Engineering, Otakaari 4, Espoo 02150, Finland

^cVTT Technical Research Centre of Finland Ltd., Nuclear Reactor Materials, Kivimiehentie 3, Espoo 02150, Finland

ARTICLE INFO

Article history:

Received 10 December 2020

Revised 19 March 2021

Accepted 27 March 2021

Available online 29 March 2021

Keywords:

Heat treatment

Laser powder bed fusion

Mechanical properties

Stainless steel

Variability

ABSTRACT

Laser powder bed fusion additive manufacturing is used for demanding applications in industries such as aerospace. However, machine-specific, optimized process conditions and parameters are required to assure consistent part quality. In addition, differences in supplied powder can cause variation in the mechanical properties of the final parts. In this paper, the variability in mechanical properties of 316L stainless steel produced with two different laser powder bed fusion machines from two different powder batches was studied by producing an identical set of tensile and impact toughness test specimens. The samples were subjected to stress-relieving, solution annealing and hot isostatic pressing to assess the effectiveness of standardized heat-treatments in reducing variation in the mechanical properties of the built parts. Porosity, microstructure, tensile properties, and impact toughness of the specimens were measured to study the effect of changing the material, machine, and heat treatment. The maximum differences observed between the studied machine-powder combinations were approximately 7% for tensile properties and approximately 20% for impact toughness. HIP reduced the variability in all other studied properties except elongation. All the specimens fulfil the minimum requirements set in ASTM F3184-16 for AM 316L.

© 2021 The Author(s). Published by Elsevier Ltd. This is an open access article under the CC BY license (<http://creativecommons.org/licenses/by/4.0/>).

1. Introduction

Laser powder bed fusion (L-PBF) additive manufacturing (AM) is already used for serial production for demanding applications in industries such as aerospace [1]. While some end-component users manufacture their own components in self-operated AM factories, most businesses purchase the needed components using an AM supplier network. Using a global AM supplier network is also a vital part of distributed manufacturing concepts [2], often discussed in operations management research [3]. In distributed manufacturing, product data is sent in digital form to a local manufacturing unit for on-demand production. This is especially convenient in the digital spare part business, which several companies are investigating [4] due to evident advantages in, for instance, warehousing and transportation costs and reduced lead times [5].

A major constraint for distributed manufacturing of parts using AM is that machine-specific, optimized process conditions and

parameters are required to assure consistent part quality. It has been shown for different materials, for example Inconel 625 [6], Inconel 718 [7], Maraging steel grade 300 [8], and 15-5PH [9], that the mechanical properties of the parts produced have statistically significant variability depending on the L-PBF machine used. Although the effect of many programmable process parameters on the mechanical properties of parts produced have been established [10], not all the inter-machine-related differences have been fully explored or are yet understood. Some evident machine-dependent parameters are build nesting density [11], part location on a building platform [12], shielding gas flow speed [13], laser spot characteristics [14], scanning strategies, and the so-called sky-writing settings [15], as well as certain other operator-managed process parameters. Many of these parameters further contribute to the inter-layer time, as defined by Mohr et al. [11], which was recently shown to cause differences in the quality of the parts produced. Typically, when making a purchase from an AM service provider, the buyer cannot, and often does not have the expertise to, influence these factors.

In addition, differences in the powder that the service provider is using can cause variations in the mechanical properties of the

* Corresponding author.

E-mail address: joni.reijonen@vtt.fi (J. Reijonen).

final parts [16]. Furthermore, the number of times the powder is re-used can have an effect on mechanical properties of parts produced [17]. During the past few years, new powder suppliers have entered the AM powder market, which has traditionally been dominated by the L-PBF machine manufacturers (OEMs). Due to the non-digital signature when verifying the powder used in current L-PBF equipment, an AM component buyer cannot be fully confident of product quality consistency, since an AM service provider may be tempted to use more affordable 3rd-party powders instead of validated powders from the respective OEM.

Distributed manufacturing quality control (QC) of locally produced components can be problematic. For instance, correctly calibrating the test equipment and supervising the test procedure can be both difficult and costly to organize. For L-PBF, process monitoring [18,19] has been suggested for quality control. This approach, however, requires recurring builds to be effective. In the case of unique safety critical production, only QC samples can be used to validate the component. In the majority of non-critical cases, though, established standard AM production quality is sufficient, as long as it is consistent among the different service providers using different equipment and powders.

The following questions address the AM component buyers' viewpoint and worries when utilizing AM in distributed manufacturing: Can consistent quality be reached in different production locations? How large are the possible differences in part properties between individual machines? Does the use of, for instance, 3rd-party powder cause unacceptable variations? Can post-process heat treatments mitigate possible production differences under the acceptance threshold and enable full use and business creation relying on an AM service provider network without expensive quality control processes?

Previous machine-to-machine variability studies [6,7,8,9] have shown that significant differences exist in the mechanical properties of specimens produced with different L-PBF machines. Prater et al. [7] further studied the effect of post-process heat treatments on the variability in tensile properties of Inconel 718. In their study, two L-PBF machines from the same machine vendor were used with identical process parameters and the same powder lot. They found that with hot isostatic pressing (HIP) followed by solution annealing (SA) and precipitation hardening, the variability in tensile properties was no longer statistically significant between specimens produced with the two different L-PBF machines. In a round-robin study by Ahuja et al. [9], age hardening heat treatment (H900) for 15-5PH stainless steel increased the variation in tensile properties compared to the as-built condition.

In this study, we mimic an AM purchase from random service providers that are using L-PBF machines and powders from different vendors, which would be the case in the distributed manufacturing of, for example, spare parts. When metal spare parts materials are considered, stainless steel 316L is one of the most commonly used materials in many industries [20], and it is therefore a relevant test material for this study. Identical sets of tensile and impact toughness test specimens were produced with two different sized and brand L-PBF machines using both OEM and non-OEM powders. Comprehensive characterization for the feedstock powders was done. The AM specimens were subjected to three different post-process heat treatments: stress-relieving (SR), SA, and HIP. The machines were operated by different persons following the standard commercial process defined by the machine vendors. The objective of this study was to quantify the difference in mechanical properties of 316L stainless steel when using L-PBF machines (and related process parameters) and powders from different OEMs, which could be considered a worst-case scenario regarding the differences between different AM service providers. In addition, the objective was to assess the effectiveness of stan-

dardized heat-treatments in reducing variation in the mechanical properties of L-PBF 316L.

2. Materials and methods

Two L-PBF machines, SLM 125 HL from SLM Solutions GmbH and EOS M 290 from EOS GmbH, were used to produce identical sets of tensile and impact test specimens. Both machines are equipped with one Ytterbium fiber laser having a maximum nominal output power of 400 W and having laser approximately 80 μm spot diameter at the focus. The maximum building volume in the SLM 125 HL is 125x125x125 mm and in the EOS M 290 250x250x325 mm. The part layout on the building platform is shown in Fig. 1. The build included in total ten pieces of 57 mm \times 7 mm \times 7 mm square bars for machining impact specimens, 16 pieces of 11 mm \times 110 mm cylinder bars for machining tensile specimens, and one powder container (located in the middle of the platform) for measuring the effective packing density of the powder bed. The powder container design and methodology were adapted from [21]. The test bars were manufactured in a vertical orientation directly onto the building platform, without additional support structures.

A default scanning strategy and process parameters, as defined by each machine manufacturer for 316L material, were used. For EOS, the 316L_SurfaceM291 1.10 parameter set and ceramic recoater blade were used. The layer height was 20 μm and the platform set temperature 80 $^{\circ}\text{C}$. For SLM, the 316L_SLM_MBP3.0_30_CE1_400W_Stripes_V1.1 parameter set was used, with a rubber recoater lip and layer height of 30 μm . The platform set temperature was 100 $^{\circ}\text{C}$. Argon was used as the shielding gas in both machines. The manufacturing process for both machines was processed as any commercial AM supplier would operate, that is, following the instructions in the L-PBF machine user manual. The fundamental laser parameters, such as scanning speed, laser power, and hatch distance, for the used commercial EOS parameter set are proprietary information of EOS. This does not affect the investigation, as the focus of this study is on quantifying the level of variance in mechanical properties of parts produced with two different L-PBF machines using commercially available parameter sets intended for use with 316L material, as would be the situation in distributed manufacturing by various additive manufacturing service providers. Moreover, the hypothesis of this study is that standardized heat treatments can be used to reduce or eliminate any observed differences in mechanical properties built using different machines, powders, and fundamental laser parameters.

After the build, all specimens were subjected to SR heat treatment at 650 $^{\circ}\text{C}$ for two hours in an argon atmosphere, cooled in air, and wire-cut from the platform. One-third of the specimens were further subjected to SA at 1066 $^{\circ}\text{C}$ for one hour in an argon atmosphere followed by air cooling, as per the AMS 2759 standard. The final third of the samples were HIP'd at 1150 $^{\circ}\text{C}$ for four hours in a 100 MPa argon atmosphere and cooled in the furnace to 180 $^{\circ}\text{C}$ at a rate of 100 $^{\circ}\text{C}/\text{min}$. One-third of the specimens were left in the SR condition.

For tensile testing, the round bars were machined to the specimen geometry defined in ISO 6892-1:2016, with a 5 mm diameter and 25 mm gauge length. The square bars were machined to a 10x10x55 mm V-notch impact test specimen geometry, as specified in ISO 148-1:2016. The tests were conducted using an Instron 1185 universal testing machine for tensile testing and a Losenhausenwerk-MFL 1959 with 300 J impact pendulum for impact testing in accordance with the aforementioned standards at room temperature (22 $^{\circ}\text{C}$). Five specimens per each condition were manufactured and subjected to tensile testing and three specimens to impact testing.

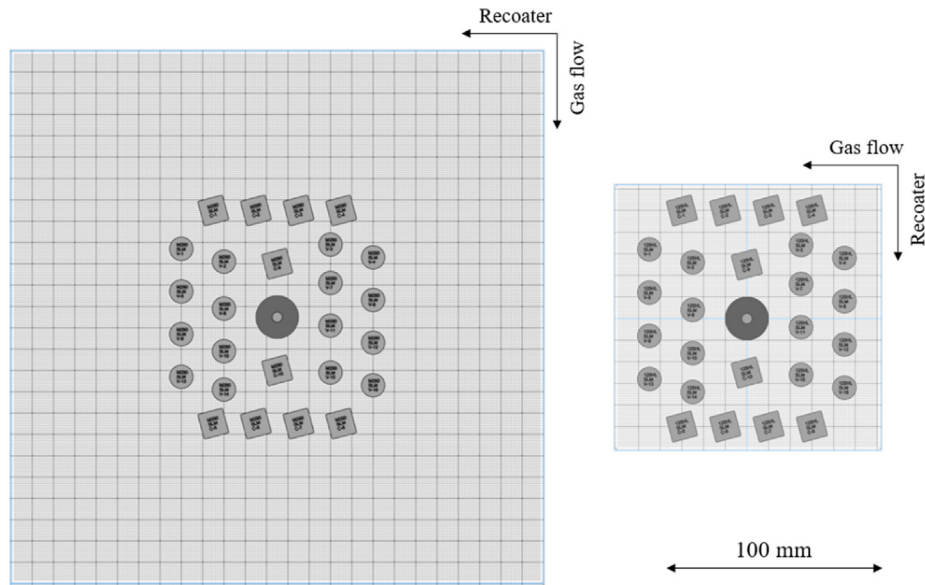


Fig. 1. The layout of test specimens on EOS M 290 (left) and SLM 125 (right) building platforms.

Cross-sections of one tensile test specimen from each condition, located in the bottom left corner of the layout in Fig. 1, were polished to a mirror finish and imaged with a ZEISS Axio Observer Inverted Microscope at a magnification of 5x. Porosity was measured from the images with image analysis using ImageJ software (Fiji, GNU license).

The same procedure was conducted on builds done with powder batches from two different vendors, having nominally the same chemical composition of 316L stainless steel. The powders were used in as-delivered condition without any additional sieving or drying procedure. The powders were characterized with SEM/EDS using a SEM 4 Zeiss Ultra Plus for particle morphology, laser diffraction using a Malvern Mastersizer 3000 for particle size distribution (PSD), and Hall-flow (ISO 4490) and Carney funnel (ASTM B964) tests for flowability.

A field emission gun-scanning electron microscope (FEG-SEM), the Zeiss Crossbeam 540 equipped with an EDAX Hikari Plus electron backscatter diffraction (EBSD) detector and solid-state four-quadrant backscatter detector (BSD), was used to characterize the fracture surface of the Charpy impact-tested specimens and the cross sections of the as-built specimens.

The fracture surface of the Charpy impact-tested specimens were analyzed using SEM-secondary electron (SE) imaging with a magnification of 20–5000x. For fractography images, the vertical upward direction is the final rupture site of the Charpy test. Inclusion chemical analysis was performed using an SEM- Energy Dispersive X-Ray (EDX). Then, SEM-EDX spectrum point analysis and area mapping were both conducted. The chemical composition was measured from the surface of the stress-relieved and machined Charpy-V samples via Optical Emission Spectroscopy using an ARL ISpark 8860. Nitrogen and Oxygen content was measured via the Carrier gas method using a Leco TC-500. One sample from each machine-powder combination was measured.

The cross-section samples of the as-built specimens were sectioned, cut with a blade saw, molded in resin, mechanically ground and polished down to 0.2 μm, and then polished with a 0.05 μm, non-crystallizing amorphous colloidal silica suspension. Detailed grain contrast images with phase information were acquired via the solid-state, four-quadrant BSD. SEM-backscatter electron (BSE) images were acquired at a magnification of 50–5000x. EBSD was conducted at magnifications of two grades (500x and 125x

with a step size of 0.3 and 1 μm, respectively). An EBSD inverted pole figure (IPF) and kernel average misorientation (KAM) images at a scale of 0–50 were analyzed using TSL OIM Analysis 8 software. In all BSD and EBSD analysis images, the AM build growth is in the horizontal direction towards the right side.

In addition, the build included a container for capturing and measuring the effective packing density of the powder in each combination of machine and powder. The packing density was measured by weighting the powder trapped inside the hollow canister during the build. The theoretical inner volume, as defined in the CAD-model, of the canister was 6.01 cm³. The true manufactured inner volume was measured by filling the canister with water.

3. Results

3.1. Powder characterization

In the Hall flow test, where the diameter of the orifice is 2.5 mm, the SLM powder had a mean flowability value of 20 s/50 g (one tap to the side of the funnel was required before each measurement to start the powder flow), while the EOS powder did not flow through the funnel at all. The Carney funnel tests, where the orifice diameter is 5 mm, gave the result of 4 s/50 g for both powders. The particle size distributions, as measured with laser diffraction (Fig. 2), show that the SLM powder has a slightly smaller average particle size compared to the EOS powder. Both powders consisted predominantly of spherical particles, as shown in the SEM images (Fig. 3). The particles in both powder batches contained satellites, but not in excessive amounts. Further SEM analysis of the polished particle cross sections revealed some internal porosity in both powders, but the number of detected pores was small (Fig. 4).

Table 1 shows the measured powder bed densities. The studied machine-powder combinations are denoted as OEM-OEMp. Apparent and tap densities measured according to ASTM B212 are also included. The EOS machine packs both powders equally, whereas a difference of approximately 5% exists in the packing density between the powders in the SLM machine. The highest packing density was seen with the combination of SLM

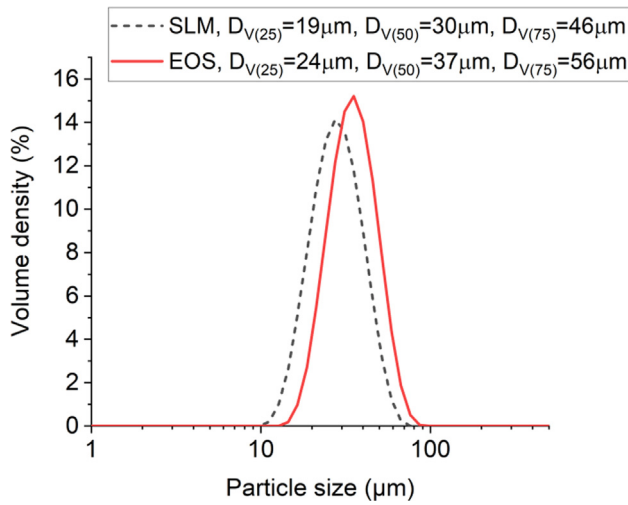


Fig. 2. Measured PSD for EOS and SLM powders.

machine and SLM powder. As can be seen from Fig. 2, the PSD of the SLM powder is smaller, which is known to result in higher tap and packing densities [22]. In Table 1, one can also notice a difference in the manufactured inner volume of the canister between the machines. This is most likely due to different scaling factors included in the parameter files of the machines.

3.2. Additive manufacturing

The printing process advanced without issues, with one exception being the build, where SLM powder was used in the EOS M 290 machine. For an unknown reason, some of the parts raised high enough above the powder bed during the process to cause an impact with the re-coater blade, temporarily stopping the process. The process was continued, and the build was finished successfully. However, the interruption caused a visible discontinuity in a few parts, two of which had to be discarded during the build (Fig. 5).

3.3. Chemical composition & porosity

The results of the chemical analysis for printed samples as well as the composition reported in the material certificates for feedstock powders are presented in Table 2. The compositions measured from printed samples are in line with the composition

reported in the material certificate and within the limits specified in the 316L AM standard ASTM F3184-16.

The measured samples generally had very low porosity values of $\leq 0.07\%$ (Fig. 6). The margin of error for the image analysis method was estimated to be approximately 0.015–0.02%, as indicated by the error bars. The results clearly show that the lower porosity values for the HIP'd samples compared to the other heat treatments were as expected. The results also indicate that the EOS machine produces more repeatable results regardless of the powder, whereas the EOS powder in the SLM machine resulted in higher porosities.

3.4. Tensile testing

The tensile samples followed ductile fracture. Fig. 7 shows the tensile testing results for each heat treatment condition. The stress-relieved state revealed maximum differences of approximately 7% in yield strength ($R_{p0.2}$), ultimate tensile strength (R_m), and elongation after fracture (A) between the machine-powder combinations. The highest tensile strengths were achieved with the SLM machine using SLM powder, and the lowest using the EOS machine with EOS powder, which in turn had the highest elongation. The variability between specimens under the same condition was small, as the error bars indicate for standard deviations.

SA reduced the R_m by 4–7%, $R_{p0.2}$ by 15–26%, while the A increased by 14–20% compared to the stress-relieved state. HIP reduced the R_m by 3–8% and the $R_{p0.2}$ by 43–47%, and it increased A by 17–32% compared to the SR condition.

All the tested specimens in each studied condition met and exceeded the minimum requirements laid out in ASTM F3184-16 for AM 316L, namely that $R_{p0.2} = 205$ MPa, $R_m = 515$ MPa, and $A = 30\%$. Within the batches of five tensile specimens for each studied condition, the standard deviations were small, 0.6–7.7 MPa for $R_{p0.2}$, 0.6–3.0 MPa for R_m , and 0.6–3.2% for A, compared to deviations of 31–50 MPa, 16–55 MPa, and 5–20%, respectively, given in material data sheets for the as-built condition for these processes [25,26].

3.5. Impact testing

Regardless of the powder and heat treatment, the specimens manufactured with the EOS machine had higher impact toughness (Fig. 8). The heat treatments reduced the impact toughness, as was the case also with the tensile strength. HIP was the most effective post treatment used in this study at reducing the variance in impact toughness caused by changing the powder or the machine. However, even after HIP the samples produced with the EOS

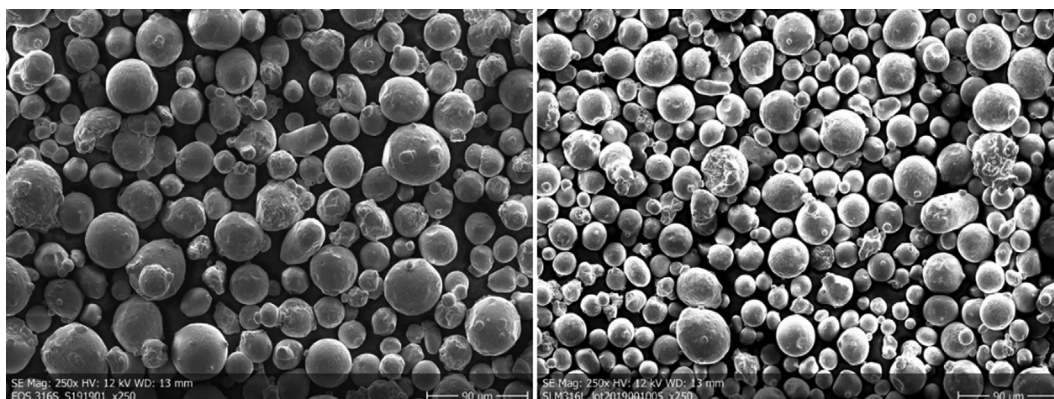


Fig. 3. SEM images showing the particle morphology of EOS (left) and SLM (right) powders.

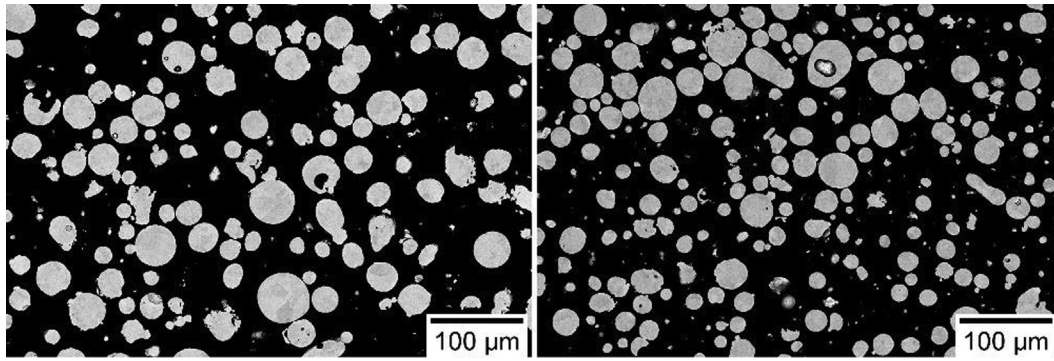


Fig. 4. Polished cross sections of EOS (left) and SLM powder (right).

Table 1
The packing density of the powder bed with the studied machine-powder combinations.

Machine-powder combination	Canister inner volume [cm ³]	Powder in canister [g]	Powder bed packing density [g/cm ³]	Apparent density [g/cm ³]	Tap density [g/cm ³]
SLM-SLMp	6.10	29.95	4.91	4.32	4.80
SLM-EOSp	6.17	28.86	4.68	4.01	4.60
EOS-EOSp	5.85	27.70	4.73	4.01	4.60
EOS-SLMp	5.82	27.61	4.74	4.32	4.80

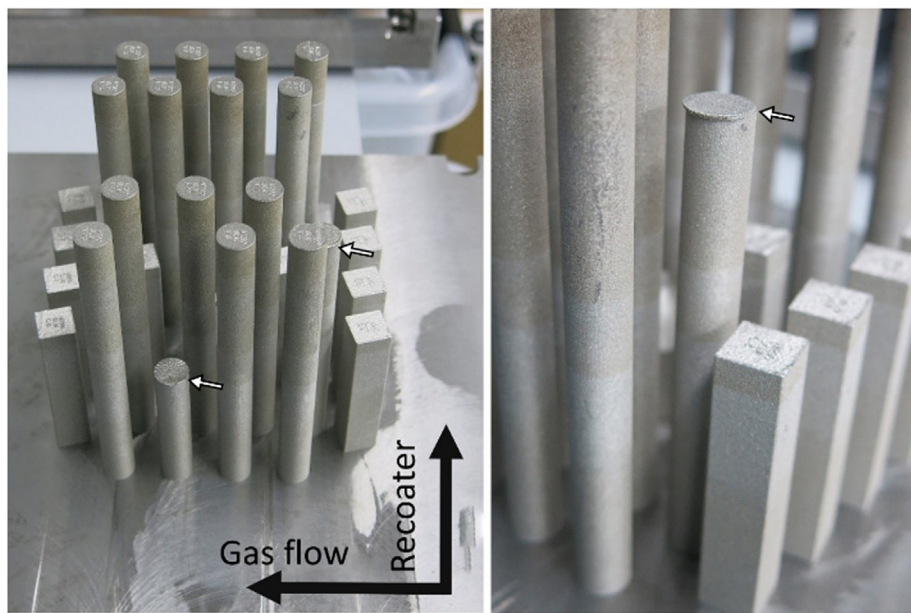


Fig. 5. Discontinuities in parts produced with EOS machine using SLM powder due to a temporary stoppage of the process.

machine had approximately a 10% higher impact toughness than those built with the SLM machine.

Lou et al. [27] have reported similar impact toughness (Charpy-V-notch) values for the AM 316L at room temperature. They reported an impact toughness values of approximately 150 J for vertically oriented samples that had been HIP'd and SA'd using the same heat treatment parameters as in this study, except for the quench medium after SA (water). Impact toughness values for wrought 316L ranged from 200 J to 350 J, and the authors concluded that the lower values for the AM specimens compared to the wrought alloy were due to a large number of oxide inclusions observed on the fracture surfaces. Controlling the oxygen content in the L-PBF process is difficult, which can result in a higher oxygen content and related oxide inclusions in finished components com-

pared to wrought parts. The difference in oxygen content in the feedstock powders and the systems' build chambers could therefore lead to a difference in the amount of oxide inclusions in the build parts. Therefore, the fracture surfaces of the impact specimens were further analyzed.

3.6. BSD & EBSD investigations

The evolution of AM 316L grain structures in SR, SA, and HIP conditions from the SLM-SLMp combination is illustrated by BSD and EBSD in Fig. 9 and Fig. 10, respectively. As implied by Fig. 9 (a, c), grains in the SR and SA conditions were mostly columnar along the built direction and highly textured. The microstructure for the SR and SA conditions was rather similar to the laminated

Table 2
Chemical compositions of printed samples, as measured with OES and powder composition and stated in the material certificates [23,24] (the values are in wt%).

Element	EOS			SLM		
	Powder (Certificate)	EOS-EOSp	SLM-EOSp	Powder (Certificate)	SLM-SLMp	EOS-SLMp
Fe	63.5	Bal.	Bal.	66.1	Bal.	Bal.
Cr	17.9	18.0	17.8	17.7	17.6	17.6
Ni	14.0	14.2	13.9	12.6	12.5	13.2
Cu	≤0.01	0.03	0.02	–	0.02	0.02
Mn	1.5	1.36	1.44	0.5	0.48	0.47
Si	0.25	0.24	0.23	0.67	0.73	0.73
Mo	2.7	3.00	2.98	2.3	2.43	2.46
Al	–	0.003	0.003	–	0.003	0.003
W	–	0.02	0.02	–	0.02	0.02
V	–	0.048	0.027	–	0.027	0.027
Ti	–	0.002	0.003	–	0.003	0.003
Co	–	0.012	0.027	–	0.013	0.027
C	0.005	<0.010	<0.010	0.016	0.010	0.010
S	0.005	0.003	0.004	0.005	0.006	0.004
P	<0.01	0.013	0.013	0.008	0.010	0.010
N	0.07	0.066	0.066	0.09	0.084	0.085
O	–	0.058	0.051	0.03	0.026	0.023

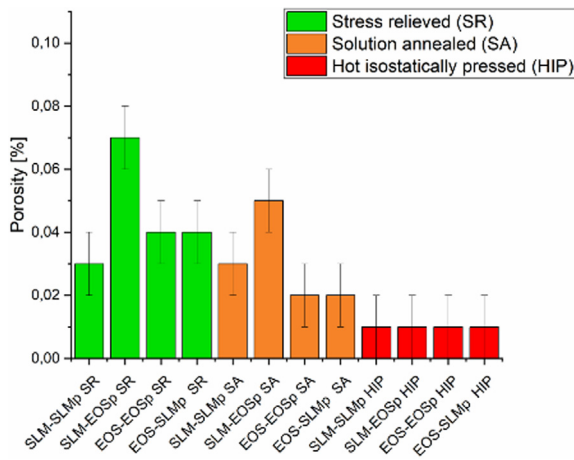


Fig. 6. Effect of machine-powder combination and heat treatment on porosity.

columnar structure (Fig. 10 (a-b, d-e)). A clear difference was observed in the HIP specimen (Fig. 9 (e)), where the annealed grains and annealing twins were observed (Fig. 10 (h)). As revealed by Fig. 10 (g), the annealed grain size was approximately 100 μm. The round inclusion particles were clearly much larger in the HIP condition than in the SA and SR conditions, as shown in Fig. 9 (b, d, f). The inclusion size in the SA condition was slightly larger than in the SR condition. KAM images with a scale of 0–5°, (shown in Fig. 10 (c, f)) indicate the release of residual strain/stress specifically inside the grains via the SA heat treatment, even though the

grain structure had not changed much from the SR condition. Fig. 10 (i) indicates that after the HIP treatment, the average misorientation increased again. After one-hour heat treatment at 1066 °C, the grains became slightly more equiaxed in the SA condition than in the SR condition (Fig. 10 (b, e)), indicating a partial recovery. The highly textured and columnar grain structure along the build direction in SR condition disappeared and equiaxed grains formed (Fig. 10 (h)) after a four-hour heat treatment at 1150 °C of HIP. However, the cellular sub-grain structure remained as seen in Fig. 9(f).

3.7. Fractography of the Charpy-V impact specimens

The SEM-SE images of the fracture surfaces of the Charpy impact-tested specimens in the SR, SA, and HIP conditions from the different machine-powder combinations are shown in Figs. 11–13 at two magnification levels. The low magnification SE images show the macroscopic fracture mode on the fracture surface, while the magnified areas exhibit the microscopic dimple details in the ductile region. Figs. 11–13 show that the dominating fracture mode is a ductile dimple fracture in all conditions, which is similar to that for wrought stainless steels. In the SLM-SLMp and SLM-EOSp combinations, a stronger formation of macrovoid and secondary cracking on the fracture surface was observed, as seen in Fig. 11 (a, c) and Fig. 12 (a). Moreover, ductile fracture more likely propagated via tearing ridges rather than microvoid coalescence in the SLM-SLMp and SLM-EOSp combinations, just as in the EOS-EOSp and EOS-SLMp combinations. Tearing ridges can be observed in Fig. 11 (b, d), Fig. 12 (d), and Fig. 13 (b). Nanometer-sized dim-

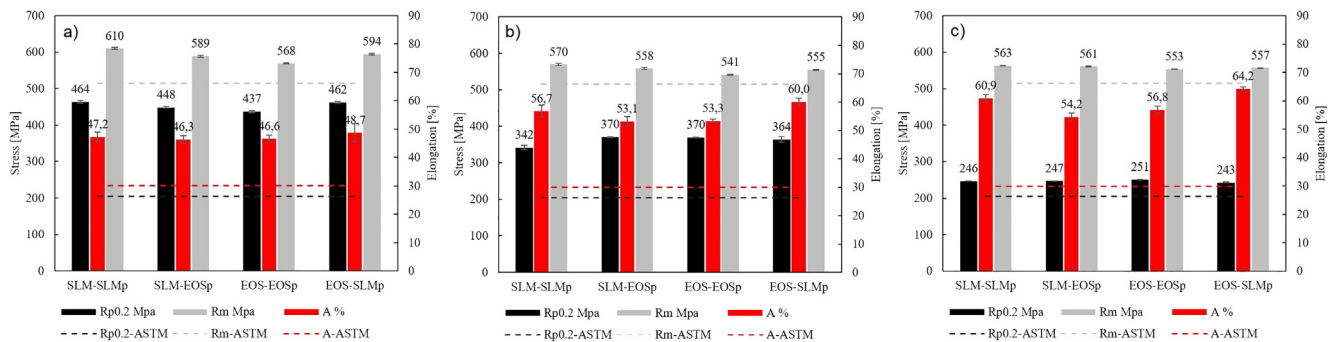


Fig. 7. Effect of machine-powder combination on Rp0.2, Rm and A in the a) SR, b) SA and c) HIP condition.

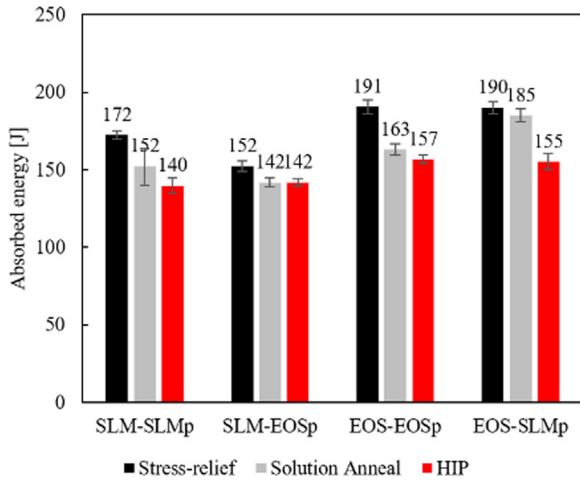


Fig. 8. Effect of machine-powder combination and heat treatment on impact toughness.

ples can be observed in Fig. 11 (f, h), Fig. 12 (b, d, f, h), and Fig. 13 (d, f, h). In general, the dimples illustrate a size difference in the three heat treatment conditions: HIP > SA > SR, which implies the coarsening of the sub-grain cellular structure and inclusions. Intergranular-like fracture topography can be observed in Fig. 13 (a, g), with SLM-SLMp and EOS-SLMp combinations in the HIP condition.

3.8. Inclusion analysis

Figs. 14–16 show high-resolution SEM-SE images of the inclusions on the Charpy impact-tested specimens in the SR, SA and HIP conditions from the different machine-powder combinations. These images show that the L-PBF 316L material exhibited typical ductile fracture similar to that for wrought stainless steels. Inclusions were mainly discovered in the dimples. This implies that the inclusions served as initiation sites for microvoid formation and coalescence [27]. In general, the size of the inclusions in the three heat treatment conditions had the following sequence: HIP

(400–1600 nm) > SA (300–600 nm) > SR (50–300 nm), showing that higher temperature heat treatments increased the oxide size. Similar oxide coarsening during high temperature heat treatments was observed by Lou et al. [27]. A larger oxide inclusion size in SLM-SLMp and EOS-SLMp combinations compared to EOS-EOSp and SLM-EOSp combinations were found, as shown in Figs. 14–16. The inclusions were oval-shaped or spherical oxides for SLM powder in both the SLM and EOS machines under SR and SA conditions (Fig. 14 (b, h) and Fig. 15 (b, h)). The inclusions were more irregular shaped, like octahedron or dodecahedron, for the EOS powder (Fig. 15 (d, f) and Fig. 16 (d, f)).

Semi-quantitative EDS chemical compositions point analysis was conducted on the selected inclusion particles marked with a red arrow in the respective SEM-SE images, with the results summarized in Table 3. EDS point analysis confirmed that the oxide inclusion particles were mostly enriched in the Si, Mo, and Mn contents. Some oxide particles also contained Al. Inclusions of specimens using SLM powder have a higher Si content and lower Mn content compared to those using EOS powder. As previously demonstrated in the chemical composition analysis, the EOS powder has a slightly higher Mn content and lower Si content than the SLM powder, which is consistent with the EDS analysis. The larger inclusion size found in the dimples fabricated from SLM powders was most probably due to the higher Si content, which has a strong affinity and fast reaction rate with oxygen in the heat treatment temperatures used.

The SLM-SLMp and EOS-SLMp combinations in the HIP condition resulted in an obvious mixed type of inclusions, as shown in Fig. 16 (b, h). The globular and darker oxides contain a higher Si content (J, N in Fig. 16 (b, h)), whereas the angular and whiter looking parts have higher Mo and Mn contents (I, M in Fig. 16 (b, h)). According to the composition and morphology, the angular, whiter looking oxide should be spinel, containing Mo, Mn and Fe, while the spherical darker oxides should be silicate.

EDS area mapping and the corresponding images from the SLM-SLMp combination in the HIP condition are shown in Fig. 17. The areas revealed oxides enriched in Si content. In addition, Mo-Mn-Cr signal in the angular regions were discovered. The area mapping confirms the angular, spherical, whiter looking Mo-Mn-Fe spinel and the spherical, darker looking silicate.

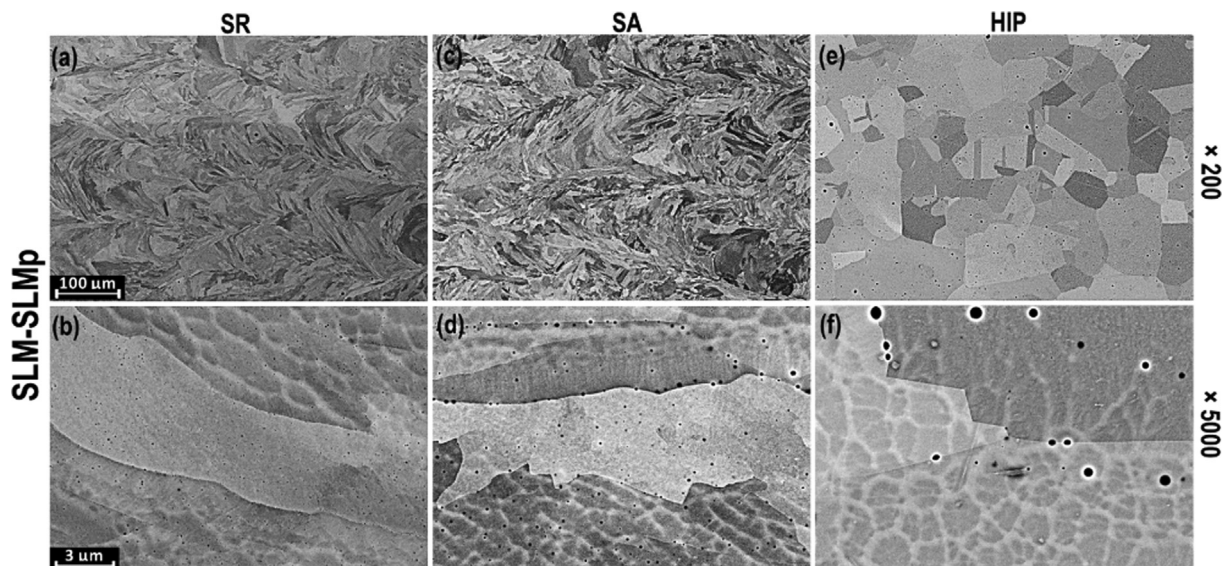


Fig. 9. SEM-BSE images of specimen cross section in SR, SA, and HIP conditions from the SLM-SLMp combination. The L-PBF build growth direction is horizontal towards right side.

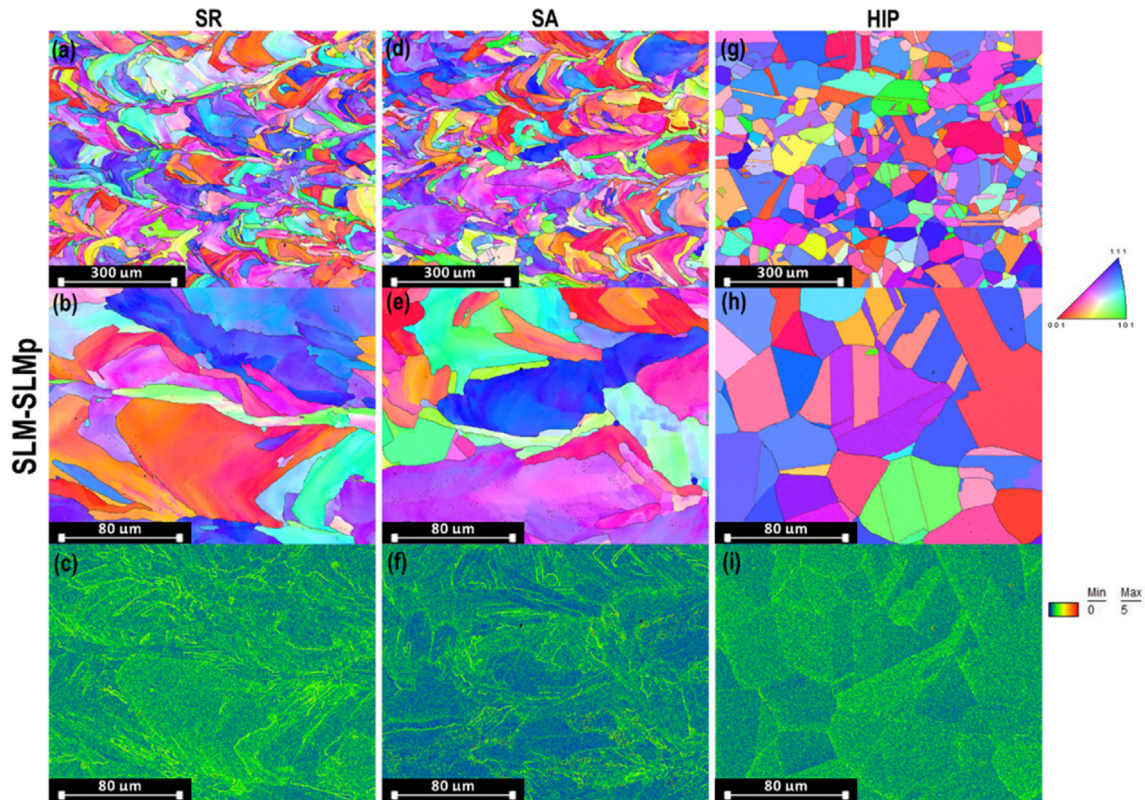


Fig. 10. EBSD images of specimen cross section in SR, SA, and HIP conditions from the SLM-SLMp combination. The L-PBF build growth direction is horizontal towards the right side.

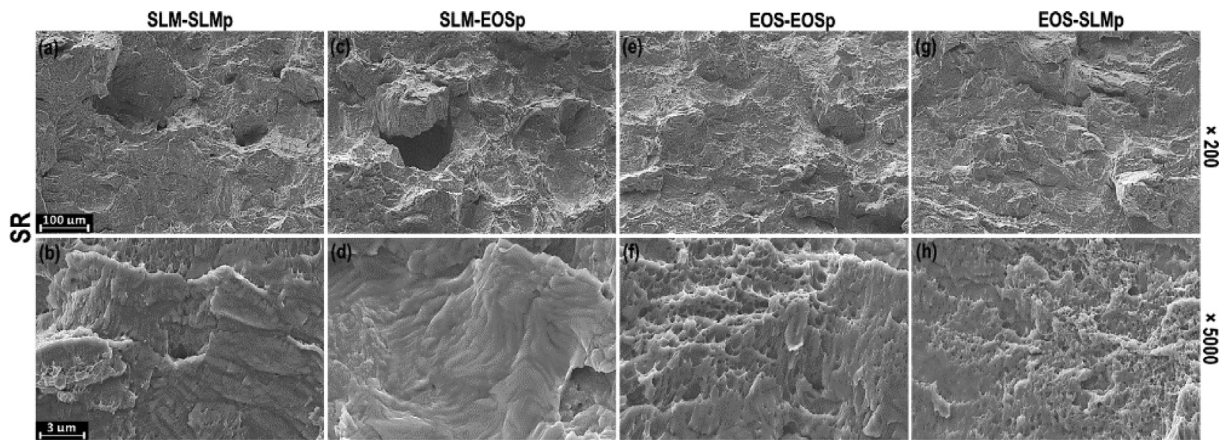


Fig. 11. SEM-SE images of the fractography of Charpy-tested specimens in the SR condition from the different machine-powder combinations. The vertical upward direction is the final rupture site.

3.9. Variability

The main hypothesis in this study was that standardized heat treatments can be used to reduce the variability in mechanical properties of AM 316L. Fig. 18 shows the coefficient of variation (CV) within each heat treatment condition calculated for all the studied mechanical properties. HIP significantly reduced the CV between the conditions for all other properties except elongation. SA reduced CV in R_m and density, but the CV increased compared to the SR condition for $R_{p0.2}$, impact toughness, and elongation. This indicates that the used SA cycle had little-to-no impact on reducing the CV. It is also important to notice that while heat treatments can be used to reduce variability in the properties, partial or

complete re-crystallization of the AM 316L microstructure during high temperature heat treatments (SA, HIP) will also reduce the tensile strength and toughness due to the loss of the extremely fine, cellular microstructure of the as-built condition.

4. Discussion

It must be kept in mind that both powders used in this study were high-quality powders intended and optimized by the respective machine manufacturers for use in L-PBF AM. The results may not apply if lower quality powders or powders with significantly different PSD not designed for use in L-PBF AM are used. In the Hall

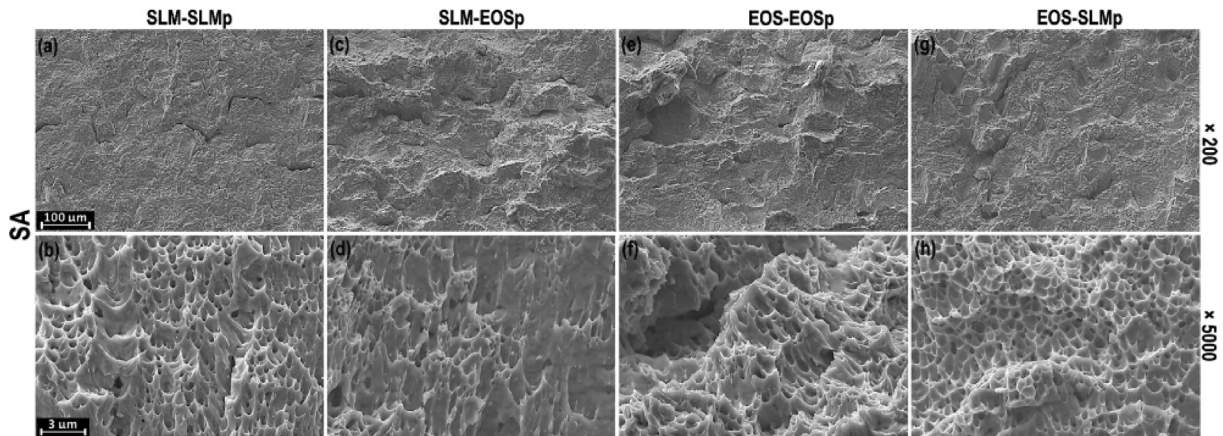


Fig. 12. SEM-SE images of the fractography of Charpy-tested specimens in the SA condition from the different machine-powder combinations. The vertical upward direction is the final rupture site.

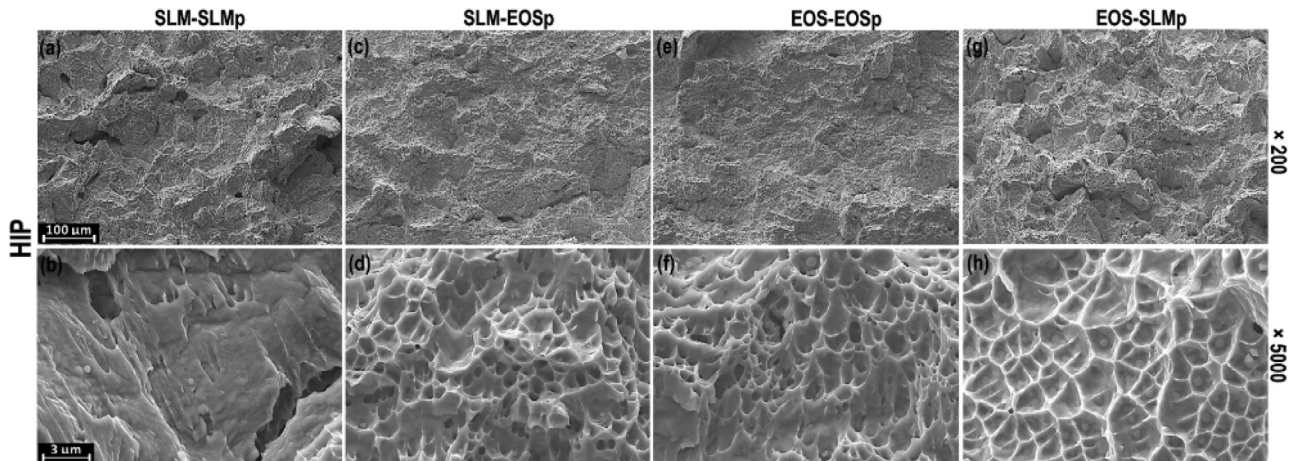


Fig. 13. SEM-SE images of the fractography of Charpy-tested specimens in the HIP condition from the different machine-powder combinations. The vertical upward direction is the final rupture site.

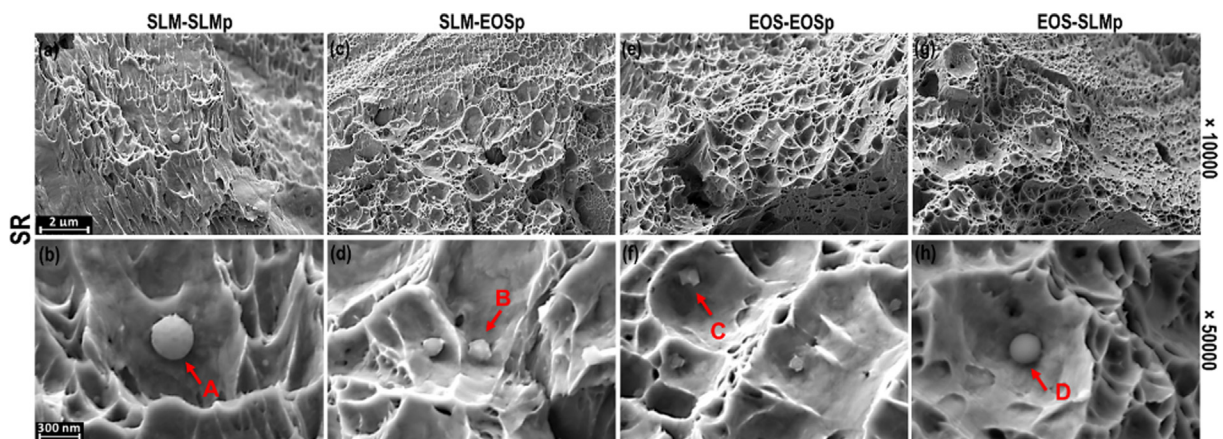


Fig. 14. SEM-SE images of the inclusions on the Charpy-tested specimens in the SR condition from the different machine-powder combinations.

flow test, the EOS powder did not flow through the funnel at all, whereas both powders performed equally when using the Carney flow test. Based on machine operators' observations, the powders spread evenly throughout both machines during the printing stage, demonstrating that the Hall flow test does not provide sufficient information on the flow properties in the powder bed process. This

deficiency has been acknowledged in previous studies, and other more suitable metrics, such as the powder's avalanche angle and rheometric properties, have been suggested for quantitative assessment of the powder spreading in AM [28].

Overall, the variation in tensile properties between the studied machine-powder combinations in the SR condition was below

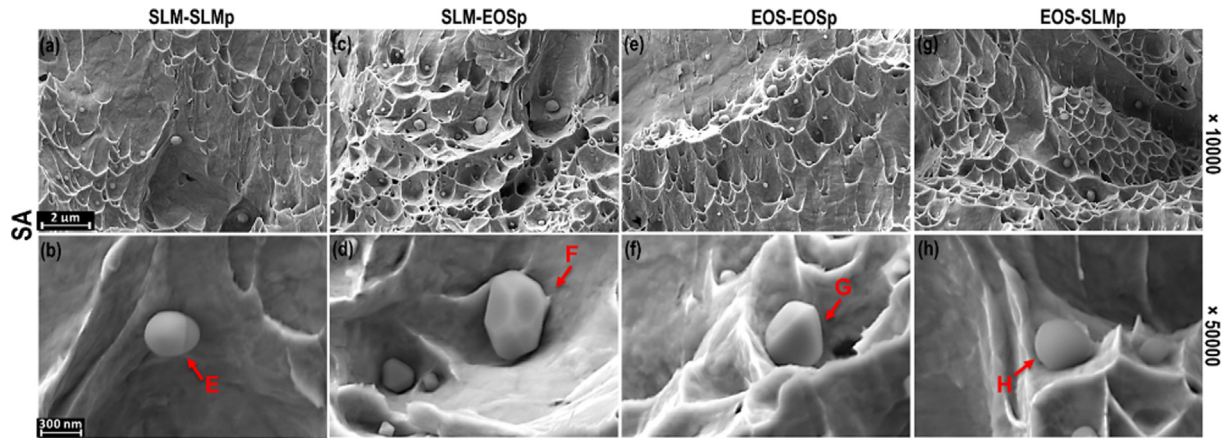


Fig. 15. SEM-SE images of the inclusions on the Charpy-tested specimens in the SA condition from the different machine-powder combinations.

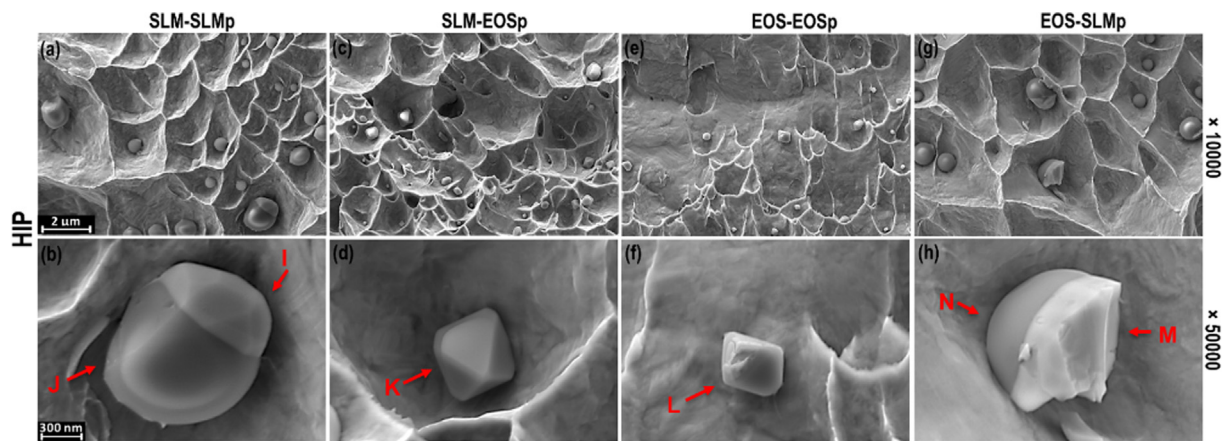


Fig. 16. SEM-SE images of the inclusions on the Charpy-tested specimens in the HIP condition from the different machine-powder combinations.

Table 3
Semi-quantitative EDS analysis (wt%) of selected points on inclusions shown in Figs. 14–16.

Condition	Specimen	Point	C	O	Al	Si	Cr	Mn	Fe	Ni	Mo
SR	SLM-SLMp	A	1.6	45.0	–	33.1	12.8	3.8	3.1	–	–
	SLM-EOSp	B	2.4	28.6	2.3	21.6	12.9	6.1	21.8	4.0	<1
	EOS-EOSp	C	2.2	37.2	2.1	6.6	25.2	7.5	16.4	1.2	1.6
	EOS-SLMp	D	3.0	42.7	1.0	36.7	8.7	<1	5.9	<1	–
SA	SLM-SLMp	E	1.8	21.6	–	19.6	8.5	11.0	3.5	–	34.0
	SLM-EOSp	F	1.8	1.5	–	–	5.7	24.2	2.6	–	64.0
	EOS-EOSp	G	1.5	2.7	–	–	6.9	19.9	4.2	<1	64.2
	EOS-SLMp	H	1.5	43.2	1.2	43.0	6.0	–	4.3	<1	–
HIP	SLM-SLMp	I	1.1	1.9	–	<1	7.3	18.9	1.0	–	69.0
		J	–	51.6	1.3	45.9	–	–	<1	–	–
	SLM-EOSp	K	2.7	64.5	1.7	–	29.1	1.9	–	–	–
	EOS-EOSp	L	3.1	66.1	–	–	28.7	1.0	1.2	–	–
	EOS-SLMp	M	<1	2.7	–	1.6	5.9	8.9	4.7	<1	74.4
		N	1.9	39.9	2.5	31.2	6.0	2.4	<1	–	15.2

7%. For impact toughness, larger differences of up to 20% between specimens were observed. This indicates that even with a small variation in tensile properties, there might be a larger variation in impact toughness or another relevant property with respect to the functioning of the part. The relationship between L-PBF processing conditions leading to unique microstructures and resulting properties such as corrosion behavior [29] and fatigue behavior [30] has also been established. This highlights the need for more comprehensive material testing in AM than the quasi-static tensile test.

There was no clear reduction in the variability of the studied mechanical properties with SA, while with HIP the variability reduced significantly. This is partly due to the fact that the used HIP cycle effectively re-crystallizes the microstructure, whereas the used SA temperature was not enough to induce recrystallization, but more importantly, it was due to the fact that HIP reduces porosity while SA does not. Interestingly, the variation in elongation after fracture increased with SA and further with HIP. This is most likely explained by the observed growth in the inclusion size during the heat treatments. The inclusion size was largest in the

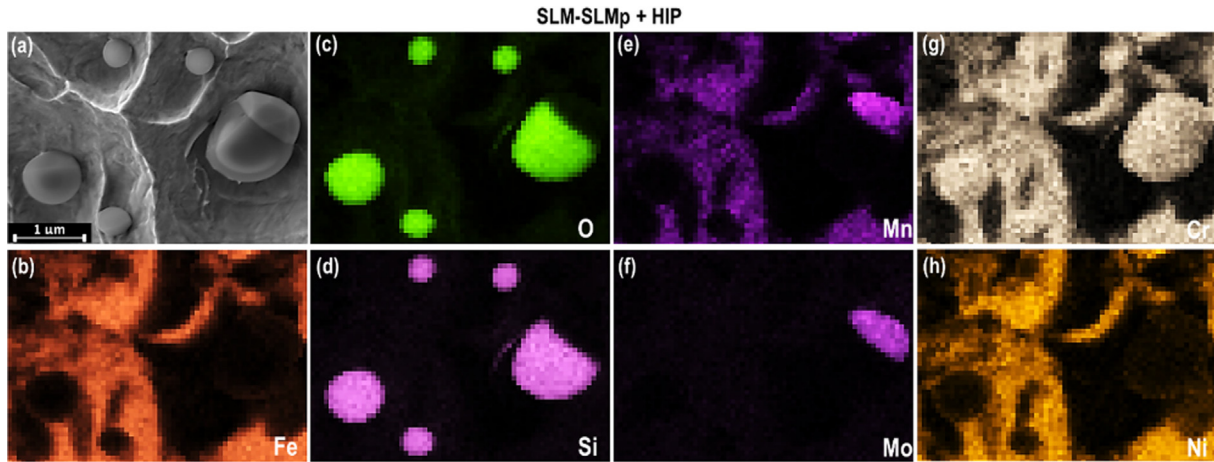


Fig. 17. EDS area analyses of the inclusions in the HIP condition from the SLM-SLMp combination.

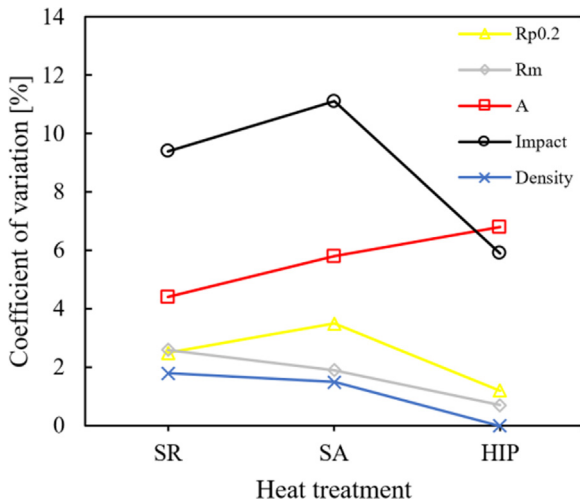


Fig. 18. Effect of heat treatment on the CV in the mechanical properties.

HIP condition, followed by SA and then SR. A similar observation regarding the wider spread in elongation after the heat treatment of L-PBF 316L was attributed to oxide inclusions also in [31].

In all the studied heat treatment conditions, the impact toughness values were higher in the specimens manufactured with the EOS machine, regardless of powder. Even after HIP, the results were approximately 10% higher than for the specimens manufactured with the SLM machine. Since the measured porosities in the HIP condition were similar between these specimens, the microstructure and fracture surfaces of the impact specimens were further analyzed.

Highly textured laminated columnar microstructure along the build direction in SR and SA conditions were found. The grains became slightly more equiaxed in the SA condition than in the SR condition, indicating a partial recovery with the release of residual strain/stress specifically inside the grains via the SA heat treatment. The highly textured and columnar grain structure along the build direction in SR condition disappeared after the HIP heat treatment, and we observed recrystallization with equiaxed grains and annealing twins where the average misorientation increased again. As seen in Fig. 9 (f), the cellular sub-grain structure remained even after HIP treatment.

This study confirmed the negative effects of Si, Mo, and Mn-rich oxide inclusions in AM 316L material on the impact toughness,

which were observed by Lou et al. [27]. The angular Mo-Mn-Fe spinel and the spherical silicate oxide inclusions promoted early microvoid formation, leading to reduced impact toughness. The higher Si content in the SLM powders appeared to cause extensive crack branching, with the formation of a higher amount of secondary cracks and the intergranular-like fracture topography in the HIP condition on the fracture surface of the Charpy impact specimens fabricated by using SLM powders. Intergranular fracture generally indicates a lower grain boundary strength, weaker grain cohesion, and lower impact energy. Oxide coarsening occurred when the AM specimens were heat treated at a high temperature, with the general inclusion size as follows: HIP (400–1600 nm) > SA (300–600 nm) > SR (50–300 nm). The coarsening of oxide inclusions and the sub-grain cellular structure also explains the increased dimple sizes in the HIP condition, since they act as initiation sites for microvoids formation and coalescence. This is in good agreement with the findings of Zhong et al., where the combined effect of the cellular structure and oxide inclusions determined the dimple size [32].

The lower impact toughness values of the AM specimens compared to wrought alloy were mainly due to the large number of oxide inclusions, which were observed and analyzed on the fracture surfaces in this study. Lou et al. have suggested that the impact toughness of AM-HIP 316L stainless steel decreases as the oxygen content increases [27], since the fracture results from a coalescence of micro-voids associated with inclusions [33]. As the oxide inclusion content increased above 0.2–0.3 vol%, the impact toughness decreased to 100–150 J. Straffelini et al. [34] have reported early tear in tensile testing due to a large amount of oxides in sintered 316L stainless steel, showing that oxides have a crucial role in the fracture process. The oxide inclusions act as initiation sites of local damage and may thus produce an early ductile decohesion, followed by dimple formation. Similar observations on the fluctuation and deterioration of mechanical properties due to oxide inclusions have been made in various studies [35,36,37].

It has been shown in laser-based directed energy deposition AM, that the area percentage of oxide inclusions in produced parts increases linearly with the total oxygen concentration, due to low solubility of oxygen in solid steel, leading to concentration of nearly all of the oxygen into oxides [38]. Deng et al. studied the effects of three oxygen sources in the L-PBF process chain: oxygen pickup during gas atomization of the powder, moisture during the powder storage and handling phase, and excess oxygen present in the L-PBF build chamber during laser melting. They concluded that the major contribution to oxide inclusions in L-PBF stainless steel parts is the oxygen already present from gas atomization in the

powder [39]. This finding is supported by the findings presented in this study. The EOS powder certificate does not report oxygen content for the starting powder; however, the SLM powder reported an oxygen content of 0.03 wt%. The measured oxygen content after building specimens from this powder with the SLM and EOS machines was 0.026 wt% and 0.023 wt%, respectively, showing no signs of significant oxygen pickup from the build chambers of either of the machines. As it was proposed by Lou et al. [27], controlling oxygen and high oxygen-affinity elements like Si and Mn during powder production is needed to reduce oxygen content and subsequent oxide inclusion in L-PBF parts.

Since the inclusion analysis was conducted from the open fracture surfaces of the impact specimens, some of the oxides may have fallen off the fracture surfaces during or after the impact test. Therefore, it was not possible to assess the total amount, distribution, or distances between the oxide inclusions in a given space of the material. The inclusion analysis did not provide a definite explanation for the difference in the impact toughness, despite the differences observed in the shape and size of the inclusions and the oxide coarsening in the specimens. The authors have a few possible explanations for such a difference, though. 1) If different, the number and distribution of the oxide inclusions in the specimens manufactured with the different machines could contribute to the differences observed in the impact toughness. 2) Even as the measured porosity in the HIP condition was equal (within the accuracy of the used method), higher porosities were measured in the SR and SA condition for the specimens manufactured with the SLM machine, regardless of the powder. Porosity was analyzed only from one cross-sectional image per specimen, which is not an absolute indication of the total porosity in the specimen. In the fractography analysis, greater macrovoid formation and secondary cracking were observed for the specimens manufactured with the SLM machine. This could indicate the presence of a higher amount of macrovoids (i.e., defects such as pores) in the specimens manufactured with the SLM machine, regardless of the powder. 3) The recrystallized grain size in the HIP condition was similar (approximately 50 μm) for all the machine-powder combinations. However, differences in the remains of the cellular sub-grain structure that we observed even after HIP could contribute to a difference in the impact toughness. Previous research has demonstrated that the cellular sub-grain structure formed by the segregation of alloying elements increases both strength and ductility, contributes to high hetero deformation-induced stress in L-PBF 316L [40,41] and that the cell-size can be altered with the fundamental laser parameters, such as scanning speed [42,43].

It is interesting to note that the discontinuities seen in Fig. 5 caused by the temporary stops during the build using the EOS machine with SLM powder did not result in any noticeable degradation of mechanical properties, even though one of the stops took place when manufacturing the gauge section of the tensile specimens. This would indicate that a temporary stoppage of the build process does not necessarily compromise the quality of the parts produced, assuming that the print can be continued and successfully completed, as was the case in this study.

5. Conclusions

This research study simulated how varying the AM metal powder source and L-PBF machine affect the quality of the produced components – tensile properties, powder bed density, porosity, and impact toughness. It mimicked a situation where a random AM service provider is used for distributed AM manufacturing. Additionally, the study assessed whether heat treatments increase reproducibility by lowering the variability in mechanical properties between samples. This is an essential matter for companies

aiming to benefit from the advantages of distributed AM production in their operations.

The largest difference between the studied machine-powder combinations was approximately 7% in tensile properties and approximately 20% for impact toughness in the SR condition. Both the SA and HIP condition reduce the absolute tensile strength and impact toughness compared to the SR condition. The SA cycle had no clear effect on the variability of mechanical properties, while HIP significantly reduced the variability between the studied machine-powder combinations in all other properties except elongation. Even after HIP, the specimens manufactured with the EOS machine, regardless of powder, showed higher impact toughness. Based on the data presented in this study, a definite conclusion regarding the cause of this cannot be made. A few possible explanations were given in the discussion. Regardless of the variation between the studied machine-powder combinations, every specimen fulfilled the requirements of ASTM F3184-16 for AM 316L and could therefore be used with confidence for distributed production of spare parts when conformity to the ASTM F3184-16 standard is adequate verification of quality.

Future research should focus on both the digital signature of the used material and testing a wider selection of powders available for AM service providers. In this study, both machines were single laser systems, and it would be necessary to study if moving from single laser to multi-laser systems would result in larger variations.

CRedit authorship contribution statement

Joni Reijonen: Conceptualization, Methodology, Formal analysis, Investigation, Writing - original draft, Writing - review & editing, Visualization. **Roy Björkstrand:** Conceptualization, Methodology, Investigation, Writing - original draft, Writing - review & editing. **Tuomas Riipinen:** Conceptualization, Methodology, Formal analysis, Investigation, Writing - original draft, Writing - review & editing, Visualization. **Zaiqing Que:** Methodology, Formal analysis, Investigation, Writing - original draft, Writing - review & editing, Visualization. **Sini Metsä-Kortelainen:** Conceptualization, Resources, Writing - review & editing, Supervision, Funding acquisition. **Mika Salmi:** Conceptualization, Resources, Writing - review & editing, Visualization, Supervision, Funding acquisition.

Declaration of Competing Interest

The authors declare that they have no known competing financial interests or personal relationships that could have appeared to influence the work reported in this paper.

Acknowledgements

This study was conducted under the DIVALIITO (Business Finland, grants 628/31/2018 and 632/31/2018) and Additive Manufacturing in Nuclear Power Plants (Valtion ydinjätehuoltora-hasto, grant SAFIR 23/2020) projects. The authors would like to thank Seija Kivi, Kimmo Ruusuvoori, Jorma Hietikko, Kim Widell, Mika Heikkinen, Antti Pasanen, Seppo Nurmi, Janne Peuraniemi, and Hanna-Mari Siniö for their contribution to the preparation of test specimens and material testing. Ulla Ehrnsten's comments are also gratefully acknowledged.

Data availability

The raw data required to reproduce the findings of this work are available from the corresponding author upon reasonable request.

References

- [1] GE, New manufacturing milestone: 30,000 additive fuel nozzles. <https://www.ge.com/additive/stories/new-manufacturing-milestone-30000-additive-fuel-nozzles>, 2018 (accessed 16 March 2020).
- [2] S. Ford, T. Minshall, Defining the Research Agenda for 3D Printing-Enabled Re-distributed Manufacturing, in: S. Umeda, M. Nakano, H. Mizuyama, H. Hibino, D. Kiritsis, G. von Cieminski, (Eds.), *Advances in Production Management Systems: Innovative Production Management Towards Sustainable Growth*, APMS 2015. IFIP Advances in Information and Communication Technology, vol 460. Springer, Cham, 2015, pp. 156–164. 10.1007/978-3-319-22759-7_18.
- [3] S.H. Khajavi, J. Partanen, J. Holmström, Additive manufacturing in the spare parts supply chain, *Comput. Ind. Eng.* 65 (1) (2014) 50–63, <https://doi.org/10.1016/j.compind.2013.07.008>.
- [4] A.S. Brown, Chain reaction - why additive manufacturing is about to change the supply chain, *Mech. Eng.* 140 (10) (2018) 30–35, <https://doi.org/10.1115/1.2018-OCT1>.
- [5] S. Chekurov, S. Metsä-Kortelainen, M. Salmi, I. Roda, A. Jussila, The perceived value of additively manufactured digital spare parts in industry: An empirical investigation, *Int. J. Prod. Econ.* 205 (2018) 87–97, <https://doi.org/10.1016/j.ijpe.2018.09.008>.
- [6] C.U. Brown, G. Jacob, S. Stoutdt, S. Moylan, J. Slotwinski, A. Donmez, Interlaboratory study for nickel alloy 625 made by laser powder bed fusion to quantify mechanical property variability, *J. Mater. Eng. Perform.* 25 (8) (2016) 3390–3397, <https://doi.org/10.1007/s11665-016-2169-2>.
- [7] T. Prater, W. Tilson, Z. Jones, Characterization of machine variability and progressive heat treatment in selective laser melting of inconel 718, 62nd JANNAP Joint Propulsion Conference. 2015 June 1–4; Nashville, TN, USA. 20150016255.
- [8] M. Moshiri, S. Candeo, S. Carmignato, S. Mohanty, G. Tosello, Benchmarking of laser powder bed fusion machines, *J. Manuf. Mater. Process.* 3 (4) (2019) 85, <https://doi.org/10.3390/jmmp3040085>.
- [9] B. Ahuja, A. Schaub, D. Junker, M. Karg, F. Tenner, R. Plettke, M. Merklein, M. Schmidt, A round robin study for laser beam melting in a metal powder bed, *S. Afr. J. Ind. Eng.* 27 (2) (2016) 30–42, <https://doi.org/10.7166/27-2-1201>.
- [10] J.P. Oliveira, A.D. LaLonde, J. Ma, Processing parameters in laser powder bed fusion metal additive manufacturing, *Mater. Des.* 193 (2020), <https://doi.org/10.1016/j.matdes.2020.108762>.
- [11] G. Mohr, S.J. Altenburg, K. Hilgenberg, Effects of inter layer time and build height on resulting properties of 316L stainless steel processed by laser powder bed fusion, *Addit. Manuf.* 32 (2020), <https://doi.org/10.1016/j.addma.2020.101080>.
- [12] A. Ladewig, G. Schlick, M. Fisser, V. Schulze, U. Glatze, Influence of the shielding gas flow on the removal of process by-products in the selective laser melting process, *Addit. Manuf.* 10 (2016) 1–9, <https://doi.org/10.1016/j.addma.2016.01.004>.
- [13] J. Reijonen, A. Revuelta, T. Riipinen, K. Ruusuvaari, P. Puukko, On the effect of shielding gas flow on porosity and melt pool geometry in laser powder bed fusion additive manufacturing, *Addit. Manuf.* 32 (2020), <https://doi.org/10.1016/j.addma.2019.101030>.
- [14] J. Metelkova, Y. Kinds, K. Kempen, C. Formanoir, A. Witvrouw, B. Van Hooreweder, On the influence of laser defocusing in Selective Laser Melting of 316L, *Addit. Manuf.* 23 (2018) 161–169, <https://doi.org/10.1016/j.addma.2018.08.006>.
- [15] A.M. Mancisidor, F. Garcandia, M. San Sebastian, P. Álvarez, J. Díaz, I. Unanue, Reduction of the residual porosity in parts manufactured by selective laser melting using skywriting and high focus offset strategies, *Phys. Procedia* 83 (2016) 864–873, <https://doi.org/10.1016/j.phpro.2016.08.090>.
- [16] A.B. Spierings, N. Herres, G. Levy, Influence of the particle size distribution on surface quality and mechanical properties in AM steel parts, *Rapid Prototyp. J.* 17 (3) (2011) 195–202, <https://doi.org/10.1108/1352541111124770>.
- [17] F. Ahmed, U. Ali, D. Sarker, E. Marzbanrad, K. Choi, Y. Mahmoodkhani, E. Toyserkani, Study of powder recycling and its effect on printed parts during laser powder-bed fusion of 17–4 PH stainless steel, *J. Mater. Process. Technol.* 278 (2020), <https://doi.org/10.1016/j.jmatprotec.2019.116522>.
- [18] A. Gögelein, A. Ladewig, G. Zenzinger, J. Bamberg, Process Monitoring of Additive Manufacturing by Using Optical Tomography, in: *Proceedings of 14th Quantitative InfraRed Thermography Conference*. 2018 25–29 June; Berlin, Germany. 266–272.
- [19] M. Bisht, N. Ray, F. Verbist, S. Coeck, Correlation of selective laser melting-melt pool events with the tensile properties of Ti-6Al-4V ELI processed by laser powder bed fusion, *Addit. Manuf.* 22 (2018) 302–306, <https://doi.org/10.1016/j.addma.2018.05.004>.
- [20] N. Kretschmar, S. Chekurov, M. Salmi, J. Tuomi, Evaluating the readiness level of additively manufactured digital spare parts: an industrial perspective, *Appl. Sci.* 8 (10) (2018) 1837, <https://doi.org/10.3390/app8101837>.
- [21] G. Jacob, A. Donmez, J. Slotwinski, S. Moylan, Measurement of powder bed density in powder bed fusion additive manufacturing processes, *Meas. Sci. Technol.* 27 (2016), <https://doi.org/10.1088/0957-0233/27/11/115601>.
- [22] B. Liu, R. Wildman, C. Tuck, I. Ashcroft, R. Hague, Investigation the effect of particle size distribution on processing parameters optimisation in selective laser melting process, in: *Proceedings of the 22th Annual International Solid Freeform Fabrication Symposium*. 2011 Aug 8–10; Austin, Texas, USA. 227–238.
- [23] SLM Solutions GmbH. Powder lot certificate. Stainless Steel 316L / 1.4404.
- [24] EOS GmbH. Powder lot certificate. Stainless Steel 316L / 1.4404.
- [25] SLM Solutions GmbH. Material data sheet. Stainless Steel 316L / 1.4404.
- [26] EOS GmbH. Material data sheet. EOS StainlessSteel 316L.
- [27] X. Lou, P.L. Andresen, R.B. Rebak, Oxide inclusions in laser additive manufactured stainless steel and their effects on impact toughness and stress corrosion cracking behavior, *J. Nucl. Mater.* 499 (2018) 182–190, <https://doi.org/10.1016/j.jnucmat.2017.11.036>.
- [28] Z. Snow, R. Martukanitz, S. Joshi, On the development of powder spreadability metrics and feedstock requirements for powder bed fusion additive manufacturing, *Addit. Manuf.* 28 (2019) 78–86, <https://doi.org/10.1016/j.addma.2019.04.017>.
- [29] D. Kong, C. Dong, X. Ni, L. Zhang, J. Yao, C. Man, X. Cheng, K. Xiao, X. Li, Mechanical properties and corrosion behavior of selective laser melted 316L stainless steel after different heat treatment processes, *J. Mater. Sci. Technol.* 35 (7) (2019) 1499–1507, <https://doi.org/10.1016/j.jmst.2019.03.003>.
- [30] C. Elangeswaran, A. Cutolo, G.K. Muralidharan, K. Vanmeensel, B.V. Hooreweder, Microstructural analysis and fatigue crack initiation modelling of additively manufactured 316L after different heat treatments, *Mater. Des.* 194 (2020), <https://doi.org/10.1016/j.matdes.2020.108962>.
- [31] M.L. Montero-Sistiaga, S. Nardone, C. Hautfenne, J. Van Humbeeck, Effect of heat treatment of 316L stainless steel produced by selective laser melting (SLM), in: *Proceedings of the 27th Annual International Solid Freeform Fabrication Symposium*. 2016 Aug 8–10; Austin, Texas, USA. 558–565.
- [32] Y. Zhong, L. Liu, S. Wikman, D. Cui, Z. Shen, Intragranular cellular segregation network structure strengthening 316L stainless steel prepared by selective laser melting, *J. Nucl. Mater.* 470 (2016) 170–178, <https://doi.org/10.1016/j.jnucmat.2015.12.034>.
- [33] W. Wang, S. Kelly, A metallurgical evaluation of the powder-bed laser additive manufactured 4140 steel material, *JOM* 68 (3) (2016) 869–875, <https://doi.org/10.1007/s11837-015-1804-y>.
- [34] G. Straffelini, V. Fontanari, A. Molinari, True and apparent Young's modulus in ferrous porous alloys, *Mater. Sci. Eng. A* 260 (1–2) (1999) 197–202, [https://doi.org/10.1016/S0921-5093\(98\)00960-5](https://doi.org/10.1016/S0921-5093(98)00960-5).
- [35] M. Lima, S. Snakaré, Microstructure and mechanical behavior of laser additive manufactured AISI 316 stainless steel stringers, *Mater. Des.* 55 (2014) 526–532, <https://doi.org/10.1016/j.matdes.2013.10.016>.
- [36] X. Zhang, Q. Zhou, K. Wang, Y. Peng, J. Ding, J. Kong, S. Williams, Study on microstructure and tensile properties of high nitrogen Cr-Mn steel processed by CMT wire and arc additive manufacturing, *Mater. Des.* 166 (2019), <https://doi.org/10.1016/j.matdes.2019.107611>.
- [37] F. Yan, W. Xiong, E. Faierson, G.B. Olson, Characterization of nano-scale oxides in austenitic stainless steel processed by powder bed fusion, *Scr. Mater.* 155 (2018) 104–108, <https://doi.org/10.1016/j.scriptamat.2018.06.011>.
- [38] M. Song, X. Lin, F. Liu, H. Yang, W. Huang, Effect of environmental oxygen content on the oxide inclusion in laser solid formed AISI 420 stainless steel, *Mater. Des.* 90 (2016) 459–467, <https://doi.org/10.1016/j.matdes.2015.11.003>.
- [39] P. Deng, M. Karadge, R.B. Rebak, V.K. Gupta, B.C. Prorok, X. Lou, The origin and formation of oxygen inclusions in austenitic stainless steels manufactured by laser powder bed fusion, *Addit. Manuf.* 35, 101334. 10.1016/j.addma.2020.101334.
- [40] W. Chen, T. Voisin, Y. Zhang, J.-B. Florian, C.M. Spadaccini, D.L. McDowell, T. Zhu, Y.M. Wang, Microscale residual stresses in additively manufactured stainless steel, *Nat. Commun.* 10 (2019) 4338, <https://doi.org/10.1038/s41467-019-12265-8>.
- [41] D. Kong, C. Dong, X. Ni, L. Zhang, C. Man, X. Li, Hetero-deformation-induced stress in additively manufactured 316L stainless steel, *Mater. Res. Lett.* 8 (10) (2020) 390–397, <https://doi.org/10.1080/21663831.2020.1775149>.
- [42] L. Liu, Q. Ding, Y. Zhong, J. Zou, J. Wu, Y.-L. Chiu, J. Li, Z. Zhang, Q. Yu, Z. Shen, Dislocation network in additively manufactured steel breaks strength-ductility trade-off, *Mater. Today*. 21 (4) (2018) 354–361, <https://doi.org/10.1016/j.mattod.2017.11.004>.
- [43] D. Kong, C. Dong, X. Ni, L. Zhang, X. Li, Cellular size dependence on the strength of additively manufactured austenitic stainless steel, *Mater. Lett.* 279 (2020), <https://doi.org/10.1016/j.matlet.2020.128524>.